



HAL
open science

Mechanics of compliant serial manipulator composed of dual-triangle segments

Wanda Zhao, Anatol Pashkevich, Damien Chablat, Alexandr Klimchik

► **To cite this version:**

Wanda Zhao, Anatol Pashkevich, Damien Chablat, Alexandr Klimchik. Mechanics of compliant serial manipulator composed of dual-triangle segments. *International Journal of Mechanical Engineering and Robotics Research*, 2021, 10 (4), pp.169-176. 10.18178/ijmerr.10.4.169-176 . hal-03195185

HAL Id: hal-03195185

<https://hal.science/hal-03195185v1>

Submitted on 10 Apr 2021

HAL is a multi-disciplinary open access archive for the deposit and dissemination of scientific research documents, whether they are published or not. The documents may come from teaching and research institutions in France or abroad, or from public or private research centers.

L'archive ouverte pluridisciplinaire **HAL**, est destinée au dépôt et à la diffusion de documents scientifiques de niveau recherche, publiés ou non, émanant des établissements d'enseignement et de recherche français ou étrangers, des laboratoires publics ou privés.

Mechanics of compliant serial manipulator composed of dual-triangle segments

Wanda Zhao, Anatol Pashkevich and Damien Chablat

Laboratoire des Sciences du Numérique de Nantes (LS2N), UMR CNRS 6004, Nantes, France

Email: wanda.zhao@ls2n.fr, Anatol.Pashkevich@imt-atlantique.fr, Damien.Chablat@cnrs.fr

Alexandr Klimchik

Innopolis University, Tatarstan, Russia

Email: A.Klimchik@innopolis.ru

Abstract—This paper focuses on the mechanics of a compliant serial manipulator composed of the new type of dual-triangle elastic segments. Both the analytical and numerical methods were used to find the stable and unstable equilibrium configurations of the manipulator, and to predict the corresponding manipulator shapes. The stiffness analysis was carried on for both loaded and unloaded modes, the stiffness matrices were computed using the Virtual Joint Method (VJM). The results demonstrate that either buckling or quasi-buckling phenomenon may occur under the loading if the manipulator initial configuration is straight or non-straight one. Relevant simulation results are presented at last, which confirm the theoretical study.

Index Terms—component, compliant manipulator, stiffness analysis, equilibrium, robot buckling, redundancy

I. INTRODUCTION

Currently, compliant serial manipulators are used more and more in many applications (such as inspection in constraint environment, medical fields etc.), because of their sophisticated motions and low weights. Conventional compliant manipulators are usually composed of rigid links and compliant actuators, like hinges, axles, or bearings. However, there is a lot of research in this area dealing with some new mechanical structures [1][2][3][4], which achieve compliant motions through tensegrity mechanisms. And one of them will be studied here.

In general, the robotic manipulators are usually classified into three types [5], conventional discrete, serpentine, and continuum robots. The first one is made of traditional rigid components. The second one uses discrete joints but combine very short rigid links with large density joints, which produce smooth curves and make the robot similar to a snake or elephant trunk [6]. While the continuum robots do not contain any rigid links or joints, they are very smooth and soft, bending continuously when working [7]. Many researchers have done studies on serpentine and continuum robots in recent years, designed flexible mechanisms for many

applications [8]. However, the pure soft continuum robot received little attention, as its small output force and design difficulty. Thus, combining rigid and elastic or soft components becomes a popular practice in designing a robot manipulator. The typical earlier hyper-redundant robot designs and implementations can be date back to the 1970s [9], which includes a series of plates interconnected by universal joints and elastic control components for pivotable action to one another. [10][11][12]

Nowadays, a very promising trend in designing compliant robots is using a series of similar segments based on various tensegrity mechanisms, which are composed in an equilibrium of compressive elements and tensile elements (cables or springs) [13][14]. Some kinds of tensegrity mechanisms have been already studied carefully. Such as [15], the authors dealt with the mechanism composed of two springs and two length-changeable bars. They analyzed the mechanism stiffness using the energy method, demonstrated that the mechanism stiffness always decreasing under external loading with the actuators locked, which may lead to “buckling”. And in [16][17], the cable-driven X-shape tensegrity structures were considered, the authors investigated the influence of cable lengths on the mechanism equilibrium configurations, which may be both stable and unstable. The relevant analysis of the equilibrium configurations stability and singularity can be seen in [18].

A new type of compliant tensegrity mechanism was proposed in our previous papers [19][20]. It is composed of two rigid triangle parts, which are connected by a passive joint in the center and two elastic edges on each side with controllable preload. The stiffness analysis of a basic dual-triangle was carried on, and the stable condition of the equilibrium was obtained. The results also showed that there may be a buckling phenomenon. Usually, while designing a robot, researchers always try to avoid buckling, but such behavior can make improvements in some fields [21]. So this phenomenon must be taken into account. In this paper, we study a compliant serial manipulator composed of the dual-triangle segments mentioned above, concentrate on the

equilibrium configurations and their transformations under the loading, which may be either continuous or sporadic that leading to buckling phenomenon. Both loaded and unloaded stiffness model of this manipulator were analyzed. The simulation of the manipulator behavior after buckling was obtained, which provides a good base of the design and relevant control algorithms of such manipulator

II. MECHANICS OF DUAL-TRIANGLE MECHANISM

Let us consider first a single segment of the compliant serial manipulator. It consists of two rigid triangles connected by a passive joint whose rotation is constrained by two linear springs as shown in Fig. 1. It is assumed that the mechanism geometry is described by the triangle parameters (a_1, b_1) and (a_2, b_2) , and the mechanism shape is defined by the central angle, which is adjusted through two control inputs influencing on the springs L_1 and L_2 . Let us denote the spring lengths in the non-stress state as L_1^0 and L_2^0 , and the spring stiffness coefficients k_1 and k_2 .

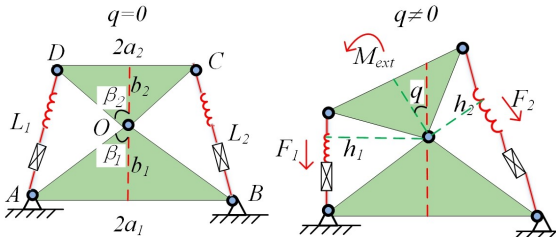


Figure 1. Geometry of a single dual-triangle mechanism.

To find the mechanism configuration angle q corresponding to the given control inputs L_1^0 and L_2^0 , let us derive first the static equilibrium equation. From Hook's law, the forces generated by the springs are $F_i = k_i(L_i - L_i^0)$ ($i = 1, 2$), where L_1 and L_2 are the spring lengths $|AD|, |BC|$. These values can be computed using the formulas $L_i(\theta_i) = \sqrt{c_1^2 + c_2^2 + 2c_1c_2 \cos(\theta_i)}$ ($i=1, 2$). Here $c_i = \sqrt{a_i^2 + b_i^2}$ ($i=1, 2$), and the angles θ_1, θ_2 are expressed via the mechanism parameters as $\theta_1 = \beta_{12} + q$, $\theta_2 = \beta_{12} - q$, and $\beta_{12} = \text{atan}(a_1/b_1) + \text{atan}(a_2/b_2)$. The torques $M_1 = F_1 \cdot h_1$, $M_2 = F_2 \cdot h_2$ in the passive joint O can be computed from the geometry, so we can get

$$\begin{aligned} M_1(q) &= +k_1(1 - L_1^0/L_1(\theta_1)) c_1 c_2 \sin(\theta_1) \\ M_2(q) &= -k_2(1 - L_2^0/L_2(\theta_2)) c_1 c_2 \sin(\theta_2), \end{aligned} \quad (1)$$

where the difference in signs is caused by the different direction of the torques generated by the forces F_1, F_2 . Further, taking into account the external torque M_{ext} applied to the moving platform, the static equilibrium equation for the considered mechanism can be written as $M_1(q) + M_2(q) + M_{\text{ext}} = 0$.

Let us now evaluate the stability of the mechanism under consideration. In general, this property highly depends on the equilibrium configuration defined by the angle q , which satisfies the equilibrium equation $M(q) +$

$M_{\text{ext}} = 0$. As follows from the relevant analysis, the function $M(q)$ can be either monotonic or non-monotonic one, so the single-segment mechanism may have multiple stable and unstable equilibriums, which are studied in detail [19][20]. As Fig. 2 shows, the torque-angle curves $M(q)$ that can be either monotonic or two-model one, the considered stability condition can be simplified and reduced to the derivative sign verification at the zero point, i.e.

$$M'(q) \Big|_{q=0} < 0 \quad (2)$$

which is easy to verify in practice. It represents the mechanism equivalent rotational stiffness for unloaded configuration with $q=0$.

Let us also consider in detail the symmetrical case, for which $a_1 = a_2 = a$, $b_1 = b_2 = b$, $k_1 = k_2$, $L_1^0 = L_2^0$. Then as follows from the mechanism geometry, to distinguish the monotonic and non-monotonic cases presented in Fig. 2, we can omit some indices and present the torque-angle relationship as well as the stiffness expression in more compact forms:

$$\begin{aligned} M(q) &= 2ck \left[c \cos \beta_{12} \sin q - L^0 \cos(\beta_{12}/2) \sin(q/2) \right] \\ M'(q) &= ck \left[2c \cos \beta_{12} \cos q - L^0 \cos(\beta_{12}/2) \cos(q/2) \right] \end{aligned} \quad (3)$$

it is also necessary to compute $M'(q)$ for unloaded equilibrium configuration $q=0$, that let us obtain the condition of the torque-angle curve monotonicity: $L^0 > 2b \cdot (1 - (a/b)^2)$ for the further analysis.

III. MECHANICS OF SERIAL MANIPULATOR

A. Manipulator Geometry and Kinematics

Let us consider a manipulator composed of three similar segments connected in series as shown in Fig. 3, where the left hand-side is fixed and the initial configuration is a "straight" one ($q_1 = q_2 = q_3 = 0$). This configuration is achieved by applying equal control inputs to all the mechanism segments. For this manipulator, it is necessary to investigate the influence of the external force $\mathbf{F}_e = (F_x, F_y)$, which causes the end-effector displacements to a new equilibrium location $(x, y)^T = (6b - \delta_x, \delta_y)^T$, which corresponds to the nonzero configuration variables (q_1, q_2, q_3) . It is also assumed here the external torque M_{ext} applied to the end-effector is equal to zero. It can be easily proved from the geometry analysis that the configuration angles satisfy the following direct kinematic equations

$$\begin{aligned} x &= b + 2bC_1 + 2bC_{12} + bC_{123} \\ y &= 2bS_1 + 2bS_{12} + bS_{123} \end{aligned} \quad (4)$$

where $C_{123} = \cos(q_1 + q_2 + q_3)$, $S_{123} = \sin(q_1 + q_2 + q_3)$, $C_{12} = \cos(q_1 + q_2)$, $S_{12} = \sin(q_1 + q_2)$, $C_1 = \cos q_1$, $S_1 = \sin q_1$. These two equations include three unknown variables, and it allows us to compute two of them if the third one was known. For instance, if the angle q_1 is

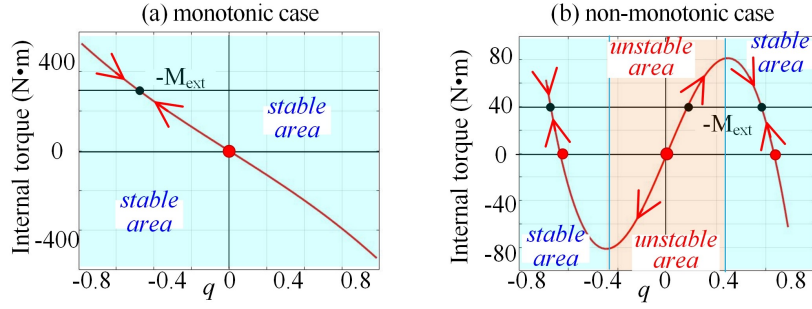


Figure 2. The torque-angle curves and static equilibria for $L_1^0 = L_2^0$ ($q_0 = 0$).

assumed to be known, the rest two angles q_2, q_3 can be computed from the classical inverse kinematics of the two-link manipulator as follows

$$\begin{aligned} q_3 &= \text{atan}(S_3/C_3) \\ q_2 &= \text{atan}\left(\frac{y-2bS_1}{x-b-2bC_1}\right) - \text{atan}\left(\frac{bS_3}{2b+bC_3}\right) - q_1 \end{aligned} \quad (5)$$

where $C_3 = \left[(x-b-2bC_1)^2 + (y-2bS_1)^2 - 5b^2 \right] / 4b^2$,

$S_3 = \pm \sqrt{1-C_3^2}$. The latter expressions provide two groups of possible solutions, which correspond to the positive/negative configuration angles $q_3 \geq 0$ and $q_3 \leq 0$.

To find a stable manipulator configuration under the loading, let us apply the energy method. It is clear that the end-effector displacement caused by the external loading leads to the deflections of mechanism springs, which allows us to compute the manipulator energy as

$$E = \frac{1}{2} \sum_{i=1}^3 \sum_{j=1}^2 k(L_{ij} - L_{ij}^0)^2 \quad (6)$$

where L_{ij} and L_{ij}^0 are the spring lengths in current and initial (unextended) states respectively. The above energy can be expressed via one of the three variables q_1, q_2 or q_3 . Assuming that variable q_1 is chosen as an independent one, the desired stable configurations can be found by computing local minima of the energy function

$$E(q_1) \rightarrow \min_{q_1} \quad (7)$$

Examples of such energy curves $E(q_1)$ for several typical cases are presented in Fig. 4.

B. Manipulator Stiffness Behavior

An alternative way to compute the configuration angles q_1, q_2, q_3 at the equilibrium state is based on the torque equation $M_e(q_1)=0$, which is implicitly used in the

energy method. The latter is illustrated by combined plots of the energy-torque curves computed for the initial “straight” configuration presented in Fig. 5, which shows that the max/min of the energy $E(q_1)$ correspond to zeros of the torque $M_e(q_1)=0$. Further, to find the external forces corresponding to this end-point location, it is necessary to use the force-torque equilibrium equation

$$\mathbf{M} + \mathbf{J}_q^T \mathbf{F} = 0 \quad (8)$$

where $\mathbf{M}=(M_{q1}, M_{q2}, M_{q3})^T$, $\mathbf{F}=(F_x, F_y, M_e)^T$. They denote the internal torques M_{q1}, M_{q2} and M_{q3} in all manipulator segments and the force/torque at the end-point. In this equation, the internal torques can be computed using the previously derived expression from section II,

$$M_{q_i} = 2k \left[(b^2 - a^2) \sin q_i - bL^0 \sin(0.5q_i) \right]; i = 1, 2, 3 \quad (9)$$

and the Jacobian matrix \mathbf{J}_q can be computed using the standard technique for the three-link manipulator presented as follows

$$\mathbf{J}_q = \begin{bmatrix} -2bS_1 - 2bS_{12} - bS_{123} & -2bS_{12} - bS_{123} & -bS_{123} \\ 2bC_1 + 2bC_{12} + bC_{123} & 2bC_{12} + bC_{123} & bC_{123} \\ 1 & 1 & 1 \end{bmatrix} \quad (10)$$

where S and C with corresponding indices have the same meaning as in (4). Assuming that the Jacobian is non-singular (i.e. the loaded manipulator is already out of the straight configuration), the external force/torque can be expressed directly as $\mathbf{F} = -\mathbf{J}_q^{-T} \mathbf{M}$, where the transport inverse matrix \mathbf{J}_q^{-T} can be computed analytically. Then we can get the following expression

$$\begin{pmatrix} F_x \\ F_y \\ M_e \end{pmatrix} = -\frac{1}{2bS_2} \begin{bmatrix} C_{12} & -C_1 - C_{12} & C_1 \\ S_{12} & -S_1 - S_{12} & S_1 \\ bS_3 & -bS_{23} - bS_3 & 2bS_2 + bS_{23} \end{bmatrix} \begin{pmatrix} M_{q1} \\ M_{q2} \\ M_{q3} \end{pmatrix} \quad (11)$$

The latter allows us to rewrite the system of the equilibrium equation (4) in the following extended form

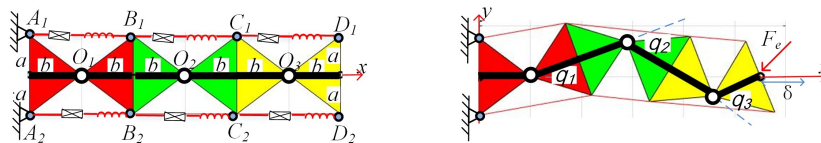


Figure 3. The torque-angle curves and static equilibria for $L_1^0 = L_2^0$ ($q_0 = 0$).

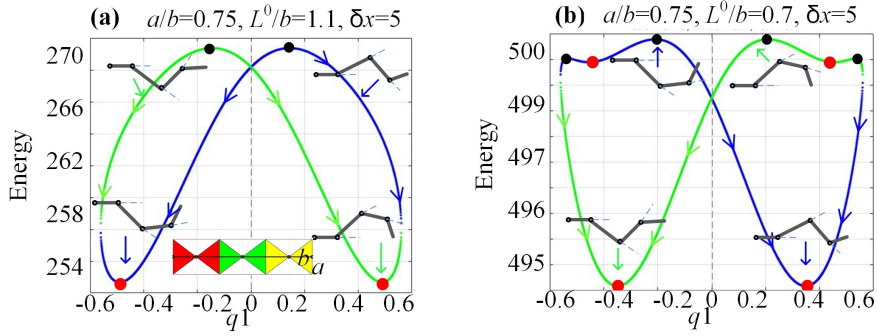


Figure 4. Energy curves $E(q_1)$ for different combinations of manipulator geometric parameters $a/b, L^0/b$:

“blue curves”— positive configuration with $q_3 > 0$; “green curves”— negative configuration with $q_3 < 0$;
 ● — stable equilibrium; ● — unstable equilibrium

$$\begin{cases} b + 2bC_1 + 2bC_{12} + bC_{123} - x = 0 \\ 2bS_1 + 2bS_{12} + bS_{123} - y = 0 \\ S_3M_{q_1} - (S_{23} + S_3)M_{q_2} + (2S_2 + S_{23})M_{q_3} = 0 \end{cases} \quad (12)$$

whose solution (q_1, q_2, q_3) may correspond to either stable or unstable equilibriums of the manipulator configuration. Then, using expressions $F_x(q_1, q_2, q_3)$ and $F_y(q_1, q_2, q_3)$ obtained from (11), one can get the external loading (F_x, F_y) corresponding to the end-effector position (x, y) , which finally allows us to generate the desired force-deflection curves. Examples of such curves for several case studies are presented in Fig. 6, where it is assumed that under the loading the manipulator moves along with x -axis, i.e. $\delta x = \text{var}$, $\delta y = 0$. As follows from this figure, in general cases (Fig. 6a), the force-deflection curves are quasi-linear, but some of them may do not pass through the zero point. The latter means that the corresponding manipulator possesses very specific particularity known as the “buckling” property [19][20][21], for which the configuration angles may suddenly change while the external force increasing gradually. Besides, in the case presented in Fig. 6b, there is the “jumping” phenomenon, because of the unstable geometrical parameters of the manipulator segment (see section II and stable condition), and the manipulator suddenly changes its shape even for extremely small loading.

To compute the critical force F_x^0 of the buckling, let us assume that the configuration angles (q_1, q_2, q_3) are small enough but not equal to zero. This allows us to derive a linearized stiffness model in the neighborhood of $q_i=0$ ($i=1, 2, 3$). Under such assumptions, the first and second equations from (3.15) can be presented in the following form

$$\begin{cases} \delta_x = b(q_1^2 + q_{12}^2 + 0.5q_{123}^2) \\ \delta_y = 2b(q_1 + q_{12} + 0.5q_{123}) \end{cases} \quad (13)$$

which allows us to present the condition $\delta_y=0$ as $q_1+q_{12}+q_{123}/2=0$. Applying similar linearization to the third equation from (12), one can get the additional relation of the configuration angles $q_1q_3 - q_2^2 + q_2q_3 + q_3^2 = 0$, which ensures the equality $M_e=0$. Further, combining these two obtained relations and considering q_2 as an independent

variable, it is possible to express q_1, q_3 in the way $q_1 = \alpha_1 \cdot q_2$, $q_3 = \alpha_3 \cdot q_2$, where

$$\alpha_1 = -(\pm\sqrt{21} + 11)/20; \quad \alpha_3 = (\pm\sqrt{21} - 1)/4 \quad (14)$$

The latter gives us four possible manipulator geometric configurations corresponding to the static equilibrium, two with U-shape and two with Z-shape (see Table 1). The corresponding external forces F_x, F_y can be linearized for small configuration angles, which yields

$$F_x \approx -\frac{k}{2bq_2} [2(b^2 - a^2) - bL^0] (q_1 + q_3 - 2q_2); F_y = 0 \quad (15)$$

Further, taking into account (13) the desired critical force can be expressed in the following way

$$F_x^o = \lim_{q_i \rightarrow 0} F_x = -\lambda \cdot \frac{k}{b} [2(b^2 - a^2) - bL^0] \quad (16)$$

where $\lambda = (\sqrt{21} - 14)/10 \approx -0.9417$ for U-shape, and $\lambda = -(\sqrt{21} + 14)/10 \approx -1.8583$ for Z-shape.

It is worth mentioning that the obtained expression allows us to derive the static stability condition for the straight configuration. In fact, this configuration is stable if and only if $F_x^o < 0$, which is equivalent to

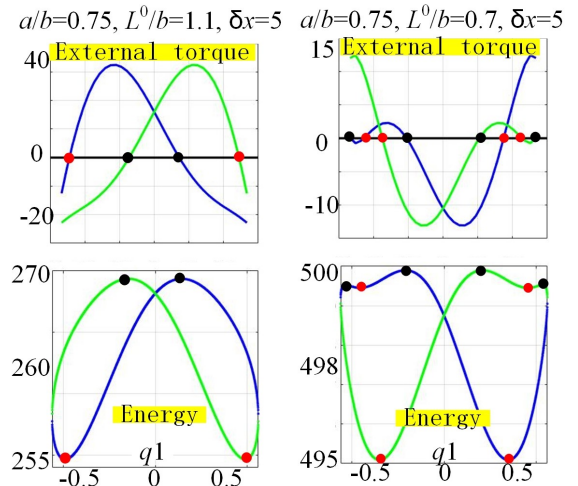


Figure 5. Correspondence between the maxima/minima of the energy curves $E(q_1)$ and zeros of the external torque $M_e(q_1)$.

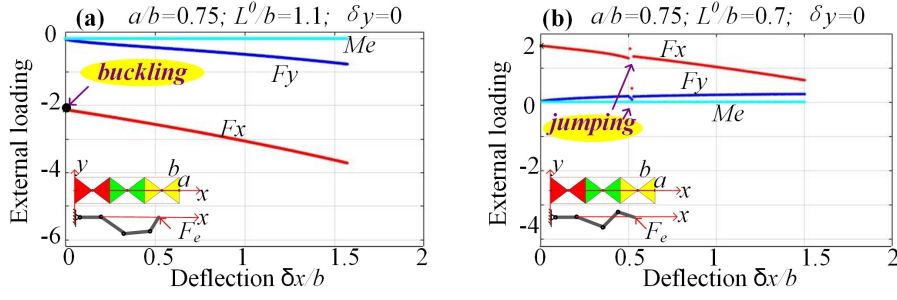


Figure 6. Force-deflection curves and stiffness coefficients for the “straight” initial configuration.

$2(b^2 - a^2) < bL^0$. It defines the monotonicity of the torque-angle curves for the manipulator segments.

Finally, let us compare the U-shape and Z-shape equilibrium configurations for their static stability. It can be easily proved that for the small configuration angles q_i , the end-effector deflection δ_x can be expressed in the following way

$$\delta_x = \mu q_2^2 \quad (17)$$

where $\mu = (\sqrt{21} + 21)/20 \approx 1.2791$ for U-shape, and $\mu = (-\sqrt{21} + 21)/20 \approx 0.8209$ for Z-shape. The latter means that for the similar deflections δ_x , the U-shape has the smaller configuration angles q_i than the one of Z-shape, which ensures smaller energy in agreement with (7).

Let us consider now when the manipulator initial configuration is non-straight, which corresponds to the angles ($q_i^0 \neq 0, i=1,2,3$). Similar to the above section, the equilibrium is defined by three equations (12), which are derived from the direct kinematics and the zero external torque assumption $M_e=0$. It can be proved that the energy curves have the “ ∞ -shape” similar to the straight configuration considered before. However, depending on the initial end-effector location (x, y) , these energy curves may be non-symmetrical and can be even discontinuous and include cusp points. Typical examples of such curves corresponding to the end-point location $(x, y)^T = (5.5b, 0)^T$ are presented in Fig. 7, where the discontinuity caused by the geometric constraint is visible. In particular, the energy curve of cases (a) consists of two separate U-shape parts that yield two symmetrical stable equilibriums and four unstable ones. Such separation is

caused by the geometric constraints $|q_i| \leq q_i^{\max}$. However, the energy curves for the case (b) cannot be treated in the same way, because the combination of a, b, L_i^0 provides non-monotonic torque-angle curves for the segments and even separate parts of the manipulator are unstable here. It should be stressed that in the cases (a), each segment of the mechanism is statically stable. It should be also noted that there are some unfeasible sections (black lines) inside of the curve, where at least one of the angles q_2 or q_3 is out of the allowable geometric limits.

The above-presented case studies, corresponding to the end-effector initial position $(x, y)^T = (5.5b, 0)^T$, can be also illustrated by the force-deflection curves presented in Fig. 8. As follows, there is no buckling phenomenon in the case (a), the curve is quasi-linear and passes through the zero point. Besides, the buckling detected in the case (b) cannot be observed in practice because of the non-stability of the separate manipulator segments.

To evaluate the manipulator stiffness matrix for the non-straight configuration, let us first find the joint torques for all manipulator segments using the method from section II,

$$M_{q_i} = 2k(b^2 - a^2)\sin(q_i) - kL_{i1}^0 [a \cos(q_i/2) + b \sin(q_i/2)] + kL_{i2}^0 [a \cos(q_i/2) - b \sin(q_i/2)]; \quad i = 1, 2, 3 \quad (18)$$

and compute the derivatives providing equivalent stiffness coefficients in the joints $K_{q_i} = dM_{q_i}/dq_i$

$$K_{q_i} = 2k(b^2 - a^2)\cos(q_i) - kL_{i1}^0 [b \cos(q_i/2) - a \sin(q_i/2)]/2 - kL_{i2}^0 [a \cdot \sin(q_i/2) + b \cos(q_i/2)]/2; \quad i = 1, 2, 3 \quad (19)$$

TABLE I. POSSIBLE MANIPULATOR SHAPES IN STATIC EQUILIBRIUM

	q1	q2	q3	Geometric configuration	Stability
Case of “+√”	−	+	+	U-shape:	Stable
	+	−	−	U-shape:	Stable
Case of “−√”	−	+	−	Z-shape:	Unstable
	+	−	+	Z-shape:	Unstable

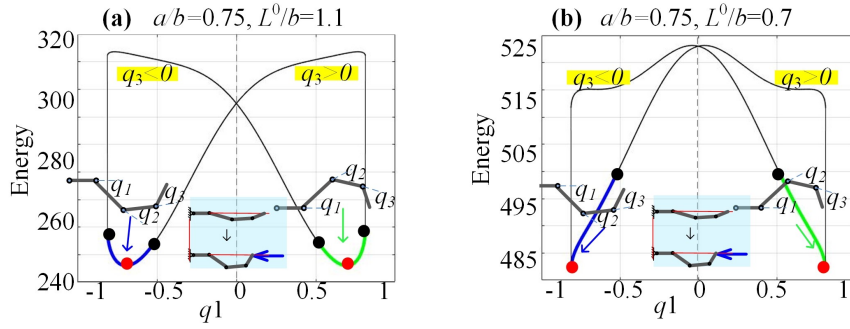


Figure 7. Energy curves $E(q_1)$ for different (a, b, L^0) for non-straight initial configuration and displacement $(\Delta x, \Delta y) = (b/2, 0)$

“blue curves” — feasible configuration with $q_3 > 0$; “green curves” — feasible configuration with $q_3 < 0$;
“black curves”— unfeasible configuration; “red point •”— stable equilibrium; “black point •”— unstable equilibrium..

This allows us to apply the VJM method and to express the unloaded stiffness matrix of the considered manipulator as

$$\mathbf{K}_F^0 = \left(\mathbf{J}_o \mathbf{K}_{q_o}^{-1} \mathbf{J}_o^T \right)^{-1} \quad (20)$$

where the subscript “o” denotes the variables corresponding to the unloaded initial configuration. Further, if we express the 2×3 submatrix of the (10) for this configuration as

$$\mathbf{J}_o = \begin{bmatrix} J_{11} & J_{12} & J_{13} \\ J_{21} & J_{22} & J_{23} \end{bmatrix}_{2 \times 3} \quad (21)$$

The desired compliance matrix of the unloaded mode can be expressed analytically in the following way

$$\mathbf{C}_F^0 = \mathbf{J}_o \mathbf{K}_{q_o}^{-1} \mathbf{J}_o^T = \begin{bmatrix} \frac{J_{11}^2}{K_{q1}} + \frac{J_{12}^2}{K_{q2}} + \frac{J_{13}^2}{K_{q3}} & * \\ * & \frac{J_{21}^2}{K_{q1}} + \frac{J_{22}^2}{K_{q2}} + \frac{J_{23}^2}{K_{q3}} \end{bmatrix} \quad (22)$$

where $\mathbf{K}_{q_o} = \text{diag}(K_{q1}, K_{q2}, K_{q3})$ is the matrix of size 3×3 .

For the loaded mode, the manipulator stiffness matrix can be computed using the extended VJM technique proposed in [22]. Within this technique, let us assume that there is a non-negligible deflection $\Delta = (\Delta x, \Delta y)^T$ caused by the external force $\mathbf{F} = (F_x, F_y)^T$, and there is a small deflection $\delta = (\delta x, \delta y)^T$ caused by this force

variation $\delta \mathbf{F} = (\delta F_x, \delta F_y)^T$ that corresponds to the joint angle variations $\delta \mathbf{q} = (\delta q_1, \delta q_2, \delta q_3)^T$. As follows from the equilibrium equation $\mathbf{M} = \mathbf{J}^T \cdot \mathbf{F}$, the corresponding variation of the joint torque can be expressed as

$$\delta \mathbf{M} = \left(\frac{d\mathbf{J}^T}{d\mathbf{q}} \delta \mathbf{q} \right) \cdot \mathbf{F} + \mathbf{J}^T \cdot \delta \mathbf{F} \quad (23)$$

where the part $d\mathbf{J}^T/d\mathbf{q}$, which includes the Jacobian derivative, can be rewritten as

$$\left(\frac{d\mathbf{J}^T}{d\mathbf{q}} \delta \mathbf{q} \right) \cdot \mathbf{F} = \sum_{i=1}^3 \left(\frac{\partial \mathbf{J}^T}{\partial q_i} \cdot \mathbf{F} \right) \delta q_i = \mathbf{K}_g \cdot \delta \mathbf{q} \quad (24)$$

where \mathbf{K}_g is the 3×3 matrix describing the influence of loading \mathbf{F} on the manipulator Jacobian \mathbf{J}

$$\mathbf{K}_g = \begin{bmatrix} \frac{\partial \mathbf{J}^T}{\partial q_1} \cdot \mathbf{F} & \frac{\partial \mathbf{J}^T}{\partial q_2} \cdot \mathbf{F} & \frac{\partial \mathbf{J}^T}{\partial q_3} \cdot \mathbf{F} \end{bmatrix}_{3 \times 3} \quad (25)$$

that can be also written in the extended form as

$$\mathbf{K}_g = \begin{bmatrix} -J_{21}F_x + J_{11}F_y & -J_{22}F_x + J_{12}F_y & -J_{23}F_x + J_{13}F_y \\ -J_{22}F_x + J_{12}F_y & -J_{22}F_x + J_{12}F_y & -J_{23}F_x + J_{13}F_y \\ -J_{23}F_x + J_{13}F_y & -J_{23}F_x + J_{13}F_y & -J_{23}F_x + J_{13}F_y \end{bmatrix}_{3 \times 3} \quad (26)$$

Further, after expressing the virtual joint torque variation as $\delta \mathbf{M} = \mathbf{K}_g \cdot \delta \mathbf{q}$ and its substitution to (23), the variable $\delta \mathbf{q}$ can be presented as

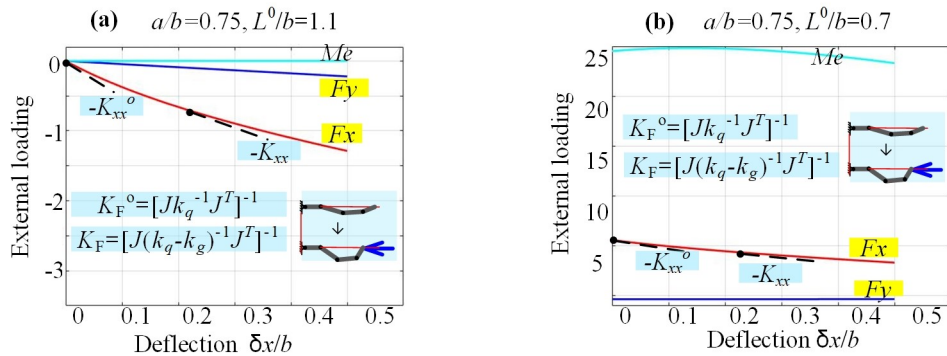


Figure 8. Force-deflection curves and stiffness coefficients for “non-straight” initial configuration with different parameters (a, b, L^0) and displacement $(\Delta x, \Delta y) = (b/2, 0)$.

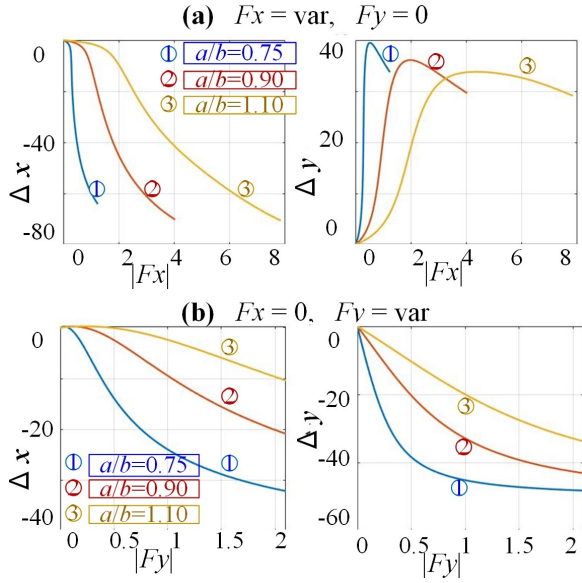


Figure 9. Force-deflection relations of three-segment mechanism for non-straight initial configuration with $(x, y)_o = (5.5b, 0)$.

$$\delta \mathbf{q} = (\mathbf{K}_q - \mathbf{K}_g)^{-1} \cdot \mathbf{J}^T \cdot \delta \mathbf{F} \quad (27)$$

which allows us to find the end-effector deflection $\delta = \mathbf{J} \cdot \delta \mathbf{q}$, and finally to obtain the desired loaded compliance and stiffness matrices

$$\mathbf{K}_F = \mathbf{J} (\mathbf{K}_q - \mathbf{K}_g)^{-1} \mathbf{J}^T \quad (28)$$

$$\mathbf{K}_F = \left[\mathbf{J} (\mathbf{K}_q - \mathbf{K}_g)^{-1} \mathbf{J}^T \right]^{-1}$$

It is worth mentioning that all the Jacobian and the joint stiffness matrices \mathbf{K}_q , \mathbf{K}_g must be computed for the loaded equilibrium configuration, which is different from the initial unloaded one (It requires relevant solutions of the non-linear equations considered above).

To illustrate the importance of the loaded stiffness analysis, the obtained expressions were applied to several cases study, which focusing on the manipulator stiffness changing under the external loading. For all considered cases, it was assumed that the initial manipulator configuration is a non-straight one, with the endpoint location $(x_0, y_0) = (5.5b, 0)$. Under the loading the configuration angles corresponding to the external force $\mathbf{F} = (F_x, F_y)^T$ were computed from (11) numerically (using

Newton's Method). There are three combinations of the geometric parameters $a/b \in \{0.75; 0.9; 1.1\}$, relevant results are presented in Figs. 9 and 10. As follows from these figures, in most cases the manipulator stiffness essentially changes if the external loading is applied. In particular, the manipulator resistance in the x -direction becomes lower and lower while the force F_x is increasing (see Fig. 9a). In contrast, the resistance in the y -direction with respect to the force F_y becomes higher and higher while this force is increasing (see Fig. 9b). These results are also confirmed by the K_{xx} and K_{yy} plots presented in Fig. 10, which show an enormous loss of x -direction resistance under the F_x loading (it can be treated as a “quasi-buckling”, see Fig. 10a for the stiffness coefficient K_{xx}). On the other side, while increasing the force F_y , the stiffness coefficient K_{yy} is very small at the beginning, then it is increasing until reaches the maximum value, and then it is decreasing (see Fig. 10b). In this figure, an evolution of the manipulator configuration under the loading are also presented, with relevant stiffness coefficients K_{xx} and K_{yy} plots (corresponding to the case $a/b=0.75$). They demonstrate the above mention results from the geometrical and physical point of view, which are corresponded to the stiffness coefficient and force relation. There are four representative configurations presented here, which showing the shapes of all segments and their position with respect to the joint limits. As follows from them, the observed sudden change of the stiffness (see Figs. 9 and 10) occurs if one of the segments is close to its joint limits, where the equivalent rotational stiffness coefficient is very low. Hence, in practice, it is necessary to avoid applying too high loading, or the manipulator will approach its joint limits and lose stiffness.

Therefore, as follows from the above study, the mechanical properties of a serial manipulator based on dual-triangle segments have several particularities, which are different from a classical serial structure composed of rigid links and compliant components. These particularities must be obligatory taken into account in control algorithm, for ensuring desired motions of such manipulator, which is in the focus of our future research.

IV. CONCLUSION

The paper focuses on the compliant serial manipulator composed of a new type of dual-triangle tensegrity mechanism, which is composed of rigid triangles

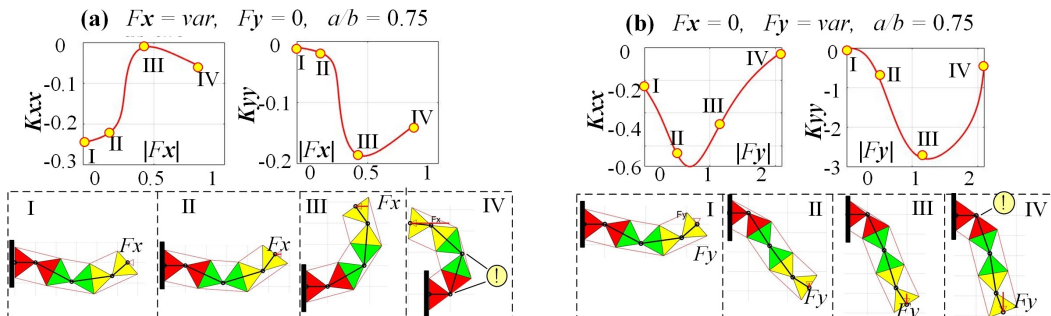


Figure 10. Evolution of the manipulator configuration under the loading.

connected by passive joints. In contrast to conventional cable-driven mechanisms, here there are two length-controllable elastic edges that can generate internal preloading. So, the mechanism can change its equilibrium configuration by adjusting the initial lengths of the elastic components.

The energy method was used to find the equilibrium configurations for different combinations of geometrical and mechanical parameters. The results show that both stable and unstable equilibria may exist, and the manipulator shape will be an essential evolution if the external loading is applied. Some analytical results are presented, which allow us to find the manipulator shape under the loading and to estimate the stability of the corresponding configuration.

The manipulator stiffness analysis for both loaded and unloaded mode was done using the VJM method, and the relations between the end-effector deflection and the external force were obtained. Similar to the single dual-triangle segment, the buckling phenomenon occurs if the manipulator initial configuration is straight. Besides, for the non-straight initial configuration, the sudden change in deflection was also observed in some cases, which was treated as quasi-buckling. These particularities of the manipulator stiffness behavior were also observed in simulation.

The obtained results allowing to predict manipulator complicated behavior under the loading, and to avoid the buckling or quasi-buckling phenomenon by proper selection of the mechanical parameters, which will be used in the future for the development of relevant control algorithms and redundancy resolution.

ACKNOWLEDGMENT

This work was supported by the China Scholarship Council (No. 201801810036).

REFERENCES

[1] M. I. Frecker, G. K. Ananthasuresh, S. Nishiwaki, N. Kikuchi, and S. Kota, "Topological Synthesis of Compliant Mechanisms Using Multi-Criteria Optimization," *Journal of Mechanical Design*, vol. 119, no. 2, pp. 238–245, Jun. 1997, doi: 10.1115/1.2826242.

[2] A. Albu-Schaffer et al., "Soft robotics," *IEEE Robotics Automation Magazine*, vol. 15, no. 3, pp. 20–30, Sep. 2008, doi: 10.1109/MRA.2008.927979.

[3] M. Y. Wang and S. Chen, "Compliant Mechanism Optimization: Analysis and Design with Intrinsic Characteristic Stiffness," *Mechanics Based Design of Structures and Machines*, vol. 37, no. 2, pp. 183–200, May 2009, doi: 10.1080/15397730902761932.

[4] L. L. Howell, "Compliant Mechanisms," in *21st Century Kinematics*, London, 2013, pp. 189–216, doi: 10.1007/978-1-4471-4510-3_7.

[5] G. Robinson and J. B. C. Davies, "Continuum robots - a state of the art," in *Proceedings 1999 IEEE International Conference on Robotics and Automation* (Cat. No.99CH36288C), May 1999, vol. 4, pp. 2849–2854 vol.4, doi: 10.1109/ROBOT.1999.774029.

[6] G. S. Chirikjian and J. W. Burdick, "Kinematically optimal hyper-redundant manipulator configurations," *IEEE Transactions on Robotics and Automation*, vol. 11, no. 6, pp. 794–806, Dec. 1995, doi: 10.1109/70.478427.

[7] J. Yang, E. P. Pitarch, J. Potratz, S. Beck, and K. Abdel-Malek, "Synthesis and analysis of a flexible elephant trunk robot,"

Advanced Robotics, vol. 20, no. 6, pp. 631–659, Jan. 2006, doi: 10.1163/156855306777361631.

[8] G. S. Chirikjian and J. W. Burdick, "A modal approach to hyper-redundant manipulator kinematics," *IEEE Transactions on Robotics and Automation*, vol. 10, no. 3, pp. 343–354, Jun. 1994, doi: 10.1109/70.294209.

[9] Anderson, Victor C., and Ronald C. Horn. "Tensor arm manipulator." U.S. Patent No. 3,497,083. 24 Feb. 1970.

[10] I. A. Gravagne and I. D. Walker, "Kinematic transformations for remotely-actuated planar continuum robots," in *Proceedings 2000 ICRA. Millennium Conference. IEEE International Conference on Robotics and Automation. Symposia Proceedings* (Cat. No.00CH37065), Apr. 2000, vol. 1, pp. 19–26 vol.1, doi: 10.1109/ROBOT.2000.844034.

[11] R. Cieślak and A. Morecki, "Elephant trunk type elastic manipulator - a tool for bulk and liquid materials transportation," *Robotica*, vol. 17, no. 1, pp. 11–16, Jan. 1999, doi: 10.1017/S0263574799001009.

[12] J. W. Hutchinson, "Postbuckling theory," p. 14.

[13] R. E. Skelton and M. C. de Oliveira, *Tensegrity systems*. Berlin: Springer, 2009.

[14] K. W. Moored, T. H. Kemp, N. E. Houle, and H. Bart-Smith, "Analytical predictions, optimization, and design of a tensegrity-based artificial pectoral fin," *International Journal of Solids and Structures*, vol. 48, no. 22–23, pp. 3142–3159, Nov. 2011, doi: 10.1016/j.ijsolstr.2011.07.008.

[15] M. Arsenaault and C. M. Gosselin, "Kinematic, static and dynamic analysis of a planar 2-DOF tensegrity mechanism," *Mechanism and Machine Theory*, vol. 41, no. 9, pp. 1072–1089, Sep. 2006, doi: 10.1016/j.mechmachtheory.2005.10.014.

[16] M. Furet, M. Lettl, and P. Wenger, "Kinematic Analysis of Planar Tensegrity 2-X Manipulators," in *Advances in Robot Kinematics 2018*, vol. 8, J. Lenarcic and V. Parenti-Castelli, Eds. Cham: Springer International Publishing, 2019, pp. 153–160.

[17] M. Furet, M. Lettl, and P. Wenger, "Kinematic Analysis of Planar Tensegrity 2-X Manipulators," in *Advances in Robot Kinematics 2018*, vol. 8, J. Lenarcic and V. Parenti-Castelli, Eds. Cham: Springer International Publishing, 2019, pp. 153–160.

[18] P. Wenger and D. Chablat, "Kinetostatic analysis and solution classification of a class of planar tensegrity mechanisms," *Robotica*, vol. 37, no. 7, pp. 1214–1224, Jul. 2019, doi: 10.1017/S026357471800070X.

[19] Zhao, W., Pashkevich, A., Klimchik, A. and Chablat, D., "Stiffness Analysis of a New Tensegrity Mechanism based on Planar Dual-triangles". In *Proceedings of the 17th International Conference on Informatics in Control, Automation and Robotics - Vol 1: ICINCO*, July, 2020, ISBN 978-989-758-442-8, pages 402-411. doi: 10.5220/0009803104020411

[20] Zhao, W., Pashkevich, A., Klimchik, A. and Chablat, D., "The Stability and Stiffness Analysis of a Dual-Triangle Planar Rotation Mechanism". In *Proceedings of ASME 2020 International Design Engineering Technical Conferences And Computers and Information in Engineering Conference IDETC/CIE*, Aug. 2020, (in press).

[21] A. Yamada, H. Mameda, H. Mochiyama, and H. Fujimoto, "A compact jumping robot utilizing snap-through buckling with bend and twist," in *2010 IEEE/RSJ International Conference on Intelligent Robots and Systems*, Taipei, Oct. 2010, pp. 389–394, doi: 10.1109/IROS.2010.5652928.

[22] S.-F. Chen and I. Kao, "Conservative Congruence Transformation for Joint and Cartesian Stiffness Matrices of Robotic Hands and Fingers," *The International Journal of Robotics Research*, vol. 19, no. 9, pp. 835–847, Sep. 2000, doi: 10.1177/02783640022067201.

Copyright © 2020 by the authors. This is an open access article distributed under the Creative Commons Attribution License ([CC BY-NC-ND 4.0](https://creativecommons.org/licenses/by-nc-nd/4.0/)), which permits use, distribution and reproduction in any medium, provided that the article is properly cited, the use is non-commercial and no modifications or adaptations are made.